Inorganic Chemistry

Article

pubs.acs.org/IC

A New Design Strategy to Access Zwitterionic Metal–Organic Frameworks from Anionic Viologen Derivates

Darpandeep Aulakh, Juby R. Varghese, and Mario Wriedt*

Department of Chemistry & Biomolecular Science, Clarkson University, 8 Clarkson Avenue, Potsdam, New York 13699, United States

Supporting Information

ABSTRACT: Two isostructural microporous zwitterionic metal–organic frameworks (ZW MOFs), $\{[M(bdcbpy)(OH_2)_4]\cdot 4H_2O\}_n$ with M = Mn (**1**) and Ni (**2**), were synthesized by the rational design of the flexible anionic viologen derivate, 1,1′-bis(3,5-dicarboxybenzyl)-4,4′-bipyridinium dibromide dihydrate solvate ($H_4bdcbpyBr_2\cdot 2H_2O$), and its self-assembly with metal(II) acetates in an aqueous medium. Single-crystal structure analyses revealed that both compounds exhibit three-dimensional hydrogen-bonded supramolecular frameworks with one-dimensional channel pores. Significantly, the pore surfaces are lined with charge gradients employed by the ZW ligand $bdcbpy^{2-}$ leading to the adsorption of hydrogen attributed to polarization effects. The thermostabilty and activation conditions were systematically investigated by thermogravimetric analysis, differential scanning calorimetry, and powder X-ray diffraction experiments. Furthermore, repeating cycles of reversible color changes are observed in air upon irradiation with UV light attributed to the formation of viologen radicals via an intermolecular electron transfer. This work also contains an in-depth literature analysis on ZW MOFs, which shows the need for the development of alternative routes for the rational design of new porous ZW MOFs.

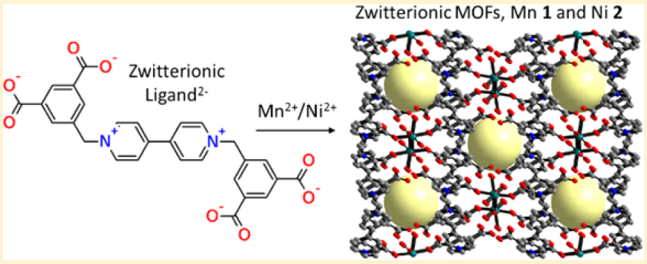

INTRODUCTION

Since the end of the 20th century, the synthesis, characterization, and functionality of metal–organic frameworks (MOFs) has become a widely researched area of study. These frameworks are crystalline porous materials built from metal clusters connected by polytypic organic linkers. An important feature is that their framework structures, pore environments, and functionalities can be controlled by the choice of metal and organic building blocks. Their primary physical properties, namely, their large accessible voids and high surface areas, offer potential applications in gas and small molecule storage.[1−3] The possibility of functionalizing their pore environments as well as tuning their topologies and pore sizes allows for their use in other diverse applications, such as chemical separation and catalysis,[4−13] with a focus on CO_2 capture in our laboratory.[14−16] Within adsorption-based applications, the most promising compounds show unique host–guest interactions based on defined binding sites through specific functional groups within the MOF cavities[17−19] and/or unsaturated metal centers.[20−22] In this context, more advanced adsorption properties are reported for a few materials showing multipoint interactions.[23,24] Even though significant research has been done in the MOF field, adsorption properties are mostly found to be based on single-point host–guest interactions that are limited to isolated areas of the pore environment. To overcome this problem, we would like to develop a different procedure with the primary objective to design materials having ideally infinite electrostatic binding sites and, thus, enhanced adsorption properties of polarizable molecules. This approach is based on a new class of MOF materials built from zwitterionic (ZW) ligands, which might have advantages over conventional MOFs.

Zwitterions (also known as betaines) are usually neutral molecules with a positively charged cationic functional group (e.g., a quaternary ammonium, phosphonium, or pyridinium N atom) and a negatively charged functional group (e.g., a carboxylate anion).[23] An electric field gradient can be found on their molecular surface due to their well-separated intramolecular charges.[24] Therefore, their incorporation in MOFs can create charged organic surfaces (COSs) within the pore environment, leading to polarization effects on guest molecules (Scheme 1). For example, albeit small, hydrogen has a finite polarizability, which enables its partial polarization in an electric field,[25] thus providing potential to form additional electrostatic interactions within the framework resulting in an enhanced adsorption enthalpy. This effect might be even more pronounced for CO_2 molecules, which are three times as polarizable and have a large quadrupole moment.[26]

Zwitterions and their complexes have been used extensively as ionic liquids in recent years as reaction media in organic synthesis and catalysis.[27−29] However, they have been rarely utilized for the purposeful design of coordination polymers or MOFs. Only a few studies have been reported so far with most

Received: November 10, 2014
Published: February 4, 2015

DOI: 10.1021/ic5026813
Inorg. Chem. 2015, 54, 1756−1764

Scheme 1. Schematic Representation of Charged Organic Surfaces in a MOF Pore

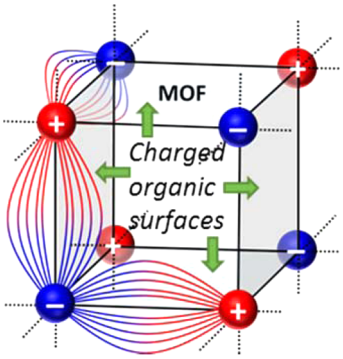

of them reporting on nonporous densely packed materials[30−36] or on potential porous materials in which charge compensation ions block the pores, leaving no void space for guest species.[37−39] In the same context, in recent years, research has been focused on new materials with interesting photochromic properties, which originate from ZW 1,1′-disubstituted-4,4′-bipyridinium-based ligands (viologens).[40−46]

To our best knowledge, only seven studies have reported porous MOFs designed through pyridnium-based ZW ligands (Scheme 2).[47−53] Kitagawa et al.[47,48] followed by Zhang et al.[50,51,53] published adsorption experiments on methanol and hydrogen. They followed a mixed ligand approach in these studies by reacting neutral ZW ligands (Scheme 2, L1 and L2) with additional conventional anionic carboxylate ligands that act as charge-compensation ions. Also, both Kitagawa et al.[52] and Shimizu et al.[49] reported on CO_2 adsorption using a cationic ZW framework built from anionic ZW ligands (Scheme 2, L3 and L4) with partially blocked pores by noncoordinating anions. To complete this overview, note that also similar ligands based organophosphonium carboxylates have been used for the synthesis of ZW MOFs as reported by Humprey et al.[54,55] In further studies different approaches for the design of ZW MOFs through non-ZW ligands are reported: Hupp et al.[56] followed a strategy in which cationic and anionic ligands were used to form a ZW framework, whereas Berke et al.[57,58] designed frameworks with dipolar surfaces based on azulene building blocks.

Scheme 2. Structural Formulas of Reported ZW Ligands Used to Design Porous MOFs[a]

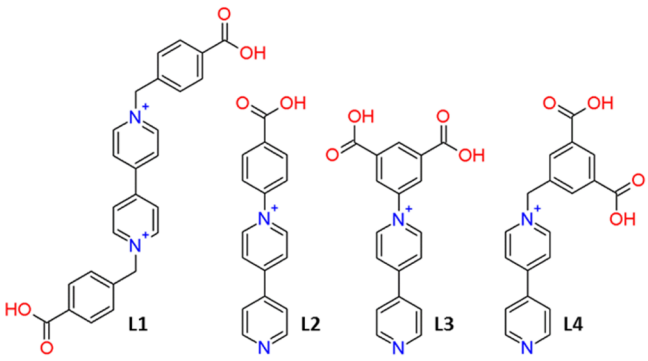

[a]Upon deprotonation L1[47,50,51] and L2[48] are neutral ligands, whereas L3[49] and L4[52] carry one negative charge.

Even though these are highly promising materials, they represent a relatively young class of compounds, and only a few of them were reported. One potential problem might have been synthetic difficulties to access these materials and their molecular building blocks. Consequently, there is no fundamental study on their structure−property relationships, which is absolutely necessary for the optimization of these materials and further development for specific applications. One of the major challenges in this field consists of the preparation of ZW MOFs without additional charge-compensating anions that might block pores to retain guest-accessible COSs. Here we report on a new strategy to access ZW MOFs by using bipyridinium-based polytopic multicharged anionic ZW ligands, which allow the rational design of ZW MOFs with no additional anions needed for the charge-compensation purpose.

EXPERIMENTAL SECTION

General Information. Commercially available reagents were used as received without further purification. Dimethyl 5-(bromomethyl) isopthalate was synthesized as previously reported.[59] The zwitterionic ligand 1,1′-bis(3,5-dicarboxybenzyl)-4,4′-bipyridinium dibromide (H_4bdcbpyBr$_2$) was synthesized as described below.

Synthesis of the Ligand 1,1′-Bis(3,5-dicarboxybenzyl)-4,4′-bipyridinium dibromide dihydrate solvate (H_4bdcbpyBr$_2$·2H$_2$O). 4,4′-bipyridine (1.56 g, 10 mmol) and 3 equiv of dimethyl 5-(bromomethyl) isopthalate were dissolved in 20 mL of acetonitrile and refluxed for 24 h at 100 °C. After the mixture was cooled to room temperature, the resulting precipitates were filtered off, washed with acetonitrile, and dried in vacuum to give Me_4bdcbpyBr$_2$ as light green powder (5.97 g, yield 82%). ^{1}H NMR (400 MHz, D_2O): δ = 9.24 (d, 2H); 8.78 (s, 1H); 8.60 (d, 2H); 8.39 (s, 2H); 6.15 (s, 2H); 4.01 (s, 3H) (Supporting Information, Figure S1: top).

Deprotection was performed by dissolving Me_4bdcbpyBr$_2$ (2.0 g) in acetic acid (50 mL) and aqueous HBr (44%, 50 mL). The solution was refluxed for 12 h and was slowly poured into 500 mL of ice water. The resulting precipitate was collected by filtration and washed with distilled water (3 × 30 mL). The filter cake was dried in vacuum and recrystallized in CH_3CN to give the product (1.44 g, yield 74%). Anal. Calcd for $C_{28}H_{26}Br_2N_2O_{10}$ (710.32): C 47.35, H 3.69, N 3.94; found: C 47.06, H 3.95, N 3.70%. IR (KBr pellet, cm^{-1}): $\tilde{\nu}$ = 3389 (w), 3123 (s), 3047 (w), 3013 (w), 2564 (w), 1700 (w), 1636 (s), 1559 (s), 1507 (s), 1449 (m), 1425 (s), 1388 (s), 1351 (m), 1296 (m), 1196 (m), 1036 (m), 876 (s), 840 (s), 805 (w), 754 (s), 718 (s), 588 (w), 512 (s), 479 (s) (Supporting Information, Figure S2). ^{1}H NMR (400 MHz, deuterated dimethyl sulfoxide (d_6-DMSO)): δ = 9.58 (d, 2H); 8.75 (d, 2H); 8.55 (s, 3H); 8.39 (s, 2H); 6.20 (s, 2H) (Supporting Information, Figure S1: bottom). ^{13}C NMR (100 MHz, d_6-DMSO): δ = 166.5, 149.8, 146.3, 135.6, 134.8, 132.7, 131.3, 127.8, 62.9 (Supporting Information, Figure S3).

Synthesis of {[Mn(bdcbpy)(OH$_2$)$_4$]·4H$_2$O}$_n$ (1). Bulk material was prepared by the following procedure: H_4bdcbpyBr$_2$·2H$_2$O (35.5 mg, 0.05 mmol) was dissolved in 1 mL of water, and the pH value of the solution was adjusted to 7 with 0.1 mol L^{-1} NaOH solution. An aqueous solution of Mn(CH$_3$COO)$_2$ (43.3 mg, 0.25 mmol) in 1 mL of water was then added to the solution. Ivory colored polycrystalline precipitate was obtained after stirring the mixture in a closed glass vial on a heating plate at 85 °C for 12 h. The residue was removed by filtration, washed with water and diethyl ether, and dried in air. The filtrate was kept to grow single crystals (see below). The purity of the bulk material was checked by powder X-ray diffraction (PXRD, Supporting Information, Figure S4: top). Yield based on the ligand: 10.1 mg (28%). Anal. Calcd for $C_{28}H_{34}MnN_2O_{16}$ (709.51): C 47.40, H 4.83, N 3.95; found: C 47.89, H 4.90, N 3.88%. IR (KBr pellet, cm^{-1}): $\tilde{\nu}$ = 3385 (w), 3122 (s), 3059 (w), 1636 (s), 1613 (s), 1559 (w), 1507 (s), 1448 (m), 1370 (w), 1241 (s), 1158 (s), 1135 (s), 840 (s), 775 (s), 719 (s), 590 (s), 493 (s) (Supporting Information, Figure S2).

DOI: 10.1021/ic5026813
Inorg. Chem. 2015, 54, 1756−1764

Single crystals suitable for X-ray structural determination were prepared in a similar fashion as described above, but the filtrate obtained in the last step was allowed to stand for several days at room temperature to give clear white block-shaped single crystals.

Synthesis of {[Ni(bdcbpy)(OH$_2$)$_4$]·4H$_2$O}$_n$ (2). Light green polycrystalline bulk material and clear light green block-shaped single crystals were prepared the same way as described above, but using Ni(CH$_3$COO)$_2$·2H$_2$O (48.7 mg, 0.25 mmol) instead of Mn(CH$_3$COO)$_2$. The purity of the bulk material was checked by PXRD (Supporting Information, Figure S4: bottom). Yield based on the ligand: 11.3 mg (32%). Anal. Calcd for $C_{28}H_{34}NiN_2O_{16}$ (713.27): C 47.15, H 4.80, N 3.93; found: C 49.60, H 4.86, N 4.14%. Note that this elemental analysis is not a close match; however, a partial dehydration of **2** to {[Ni(bdcbpy)(OH$_2$)$_4$]·3H$_2$O}$_n$ would be in rough agreement with these findings. Anal. Calcd for $C_{28}H_{32}NiN_2O_{15}$ (695.26): C 48.37, H 4.64, N 4.03%. This is supported by TGA measurements (see Thermal Properties Section). IR (KBr pellet, cm^{-1}): $\tilde{\nu}$ = 3385 (w), 3125 (s), 3058(m), 1636 (s), 1617 (m), 1560 (w), 1508 (s), 1445 (m), 1371 (w), 1242 (s), 1163 (s), 1139 (s), 840 (s), 769 (s), 721 (s), 594 (s), 497 (s) (Supporting Information, Figure S2).

Single-Crystal Structure Analysis. Data collections were performed on single crystals coated with Paratone-N oil and mounted on Kapton loops. Single-crystal X-ray data of all compounds were collected on a Bruker Kappa Apex II X-ray diffractometer outfitted with a Mo X-ray source (sealed tube, λ = 0.71073 Å) and an APEX II CCD detector equipped with an Oxford Cryosystems Desktop Cooler low-temperature device. The APEX-II software suite was used for data collection, cell refinement, and reduction.[60] Absorption corrections were applied using SADABS.[61] Space group assignments were determined by examination of systematic absences, *E*-statistics, and successive refinement of the structures. Structure solutions were performed with direct methods using SHELXT-2014, and structure refinements were performed by least-squares refinements against $|F|^2$ followed by difference Fourier synthesis using SHELXL-2014.[62−64] All non-hydrogen atoms were refined with anisotropic displacement parameters. The O−H hydrogen atoms in all compounds were located in the difference map, where the bond lengths were set to ideal values with d_{O-H} = 0.84 Å and were refined using a riding model. The C−H atoms were positioned with idealized geometry and were refined with fixed isotropic displacement parameters [U_{eq}(H) = −1.2U_{eq}(C)] using a riding model with d_{C-H} = 0.95 Å (aromatic) and 0.99 Å (methylene). Note that in **1** and **2** only one noncoordinating water molecule could be refined and that after structure refinement there were some residual peaks found in the electron density map for which no reasonable model was found. Thus, the data were corrected using the SQUEEZE option in PLATON.[65] SQUEEZE estimated a total count of 105 electrons per 281.2 Å^3 of solvent-accessible volume in **1** and 107 electrons per 284.5 Å^3 of solvent-accessible volume in **2**, which are in good agreement to be three water molecules per asymmetric unit. The overall water content of four coordinating and four noncoordinating water molecules was further confirmed by TGA and elemental analysis. Details of the structure determination are given in Table 1.

Powder X-ray Diffraction. The PXRD patterns were recorded on a Bruker D2 Phaser diffractometer equipped with a Cu sealed tube (λ = 1.54178 Å). Powder samples were dispersed on low-background discs for analyses. PXRD data of the anhydrates 1′and 2′ were collected using an airtight sample holder. Simulation of the PXRD data was carried out by using single-crystal data and the Powder Pattern module of the Mercury CSD software package.[66]

Thermogravimetric Analysis. Thermogravimetric (TG) data were recorded using a TGA Q50 from TA Instruments. All measurements were performed using platinum crucibles in a dynamic nitrogen atmosphere (50 mL/min) and a heating rate of 3 °C·min^{-1}. The instrument was corrected for buoyancy and current effects and was calibrated using standard reference materials.

Differential Scanning Calorimetry. Differential Scanning Calorimetry (DSC) data were recorded using a TGA Q20 from TA Instruments. All measurements were performed using T-zero aluminum pans, a dynamic nitrogen atmosphere (50 mL/min), and a heating rate of 3 °C·min^{-1}. The instrument was calibrated using standard reference materials.

Table 1. Selected Crystal Data and Details on the Structure Determinations from Single Crystal Data for Compounds 1 and 2

compound	1	2
formula	$C_{28}H_{34}MnN_2O_{16}$	$C_{28}H_{34}NiN_2O_{16}$
MW [g·mol^{-1}]	709.51	713.27
crystal system	monoclinic	monoclinic
space group	$P2_1/n$	$P2_1/n$
a [Å]	12.5007(2)	12.3743(7)
b [Å]	12.7914(3)	12.8620(7)
c [Å]	18.5855(5)	18.4671(10)
α [deg]	90	90
β [deg]	98.5482(9)	98.5756(19)
γ [deg]	90	90
V [Å^3]	2938.83(12)	2906.3(3)
T [K]	170(2)	170(2)
Z	4	4
D_{calc} [g·cm^{-3}]	1.481	1.507
μ [mm^{-1}]	0.520	0.739
min/max transmission	0.926/0.954	0.898/0.940
θ_{max} [deg]	28.291	28.397
measured reflections	40425	41507
unique reflections	7292	7240
reflections [$F_0 > 4\sigma(F_0)$]	4844	6095
parameter	397	397
R_{int}	0.0658	0.0367
R_1 [$F_0 > 4\sigma(F_0)$]	0.0533	0.0389
wR_2 [all data]	0.1564	0.1122
GOF	1.016	1.048
$\Delta\rho_{max}/\Delta\rho_{min}$ [e·Å^{-3}]	0.792/−0.446	0.686/−0.450

Adsorption Analysis. Gas adsorption isotherms for pressures in the range from 1 × 10^{-5} to 1.1 bar were measured by a volumetric method using a Micromeritics ASAP2020 surface area and pore analyzer. A preweighed analysis tube was charged with a sample of compounds **1** and **2**, capped and evacuated by heating at 40 °C under dynamic vacuum for 2 h. The evacuated analysis tubes containing the activated samples were then carefully transferred to an electronic balance and weighed to determine the mass of sample (37.5 mg for **1** and 60.8 mg for **2**). The tubes were then transferred to the analysis port of the gas adsorption instrument. For all isotherms, warm and cold free space correction measurements were performed using ultrahigh purity He gas (UHP grade 5.0, 99.999% purity). All gases used are UHP grade (99.999% purity). N_2 and H_2 isotherms at 77 K were measured in liquid nitrogen, and CO_2 isotherms at 195 K were measured using a dry ice/acetone bath. All temperatures and fill levels were monitored periodically throughout the measurement. Oil-free vacuum pumps and oil-free pressure regulators were used for all measurements to prevent contamination of the samples during the evacuation process or of the feed gases during the isotherm measurements.

Elemental Analysis. Elemental analyses (C, H, and N) were obtained by Atlantic Microlab, Inc.

Spectroscopy. FT-IR data were recorded on a Nicolet iS10 from Thermo Scientific. ^{1}H NMR data were recorded on Avance DMX-400 from Bruker.

RESULTS AND DISCUSSION

Synthesis of ZW MOFs through ZW Ligand Design. As outlined above, the rational design of ZW MOFs from ZW ligands has suffered so far from the incorporation of charge-balancing non-ZW anions in the framework. To overcome this problem we designed the new ZW ligand H$_4$bdcbpyBr$_2$, which

DOI: 10.1021/ic5026813
Inorg. Chem. 2015, 54, 1756−1764

Scheme 3. ZW Ligand $H_4bdcbpyBr_2$ is Synthesized through a Facile Two-Stage Reaction[a]

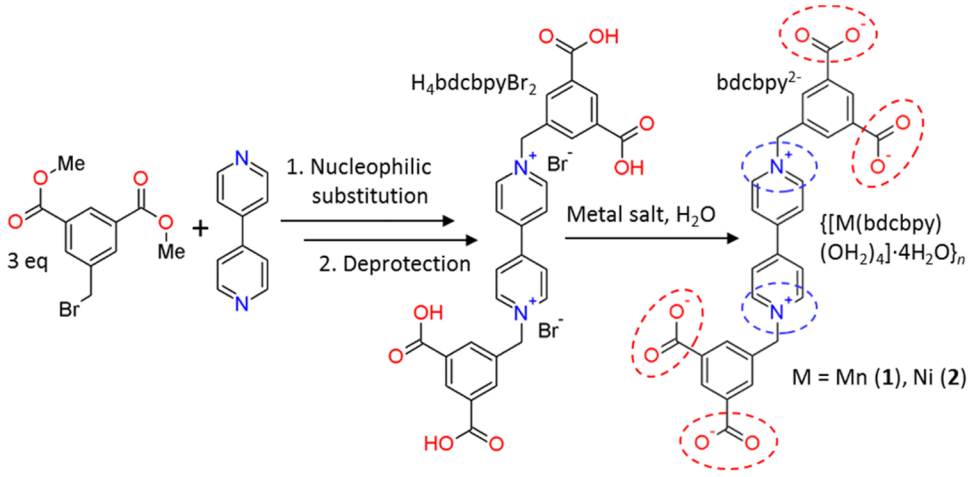

[a]Followed by its reaction with metal salts, ZW MOFs **1** and **2** are formed, while $H_4bdcbpyBr_2$ is in situ deprotonated to its anionic form $bdcbpy^{2-}$. The charges of $bdcbpy^{2-}$ are highlighted through dashed ellipsoids.

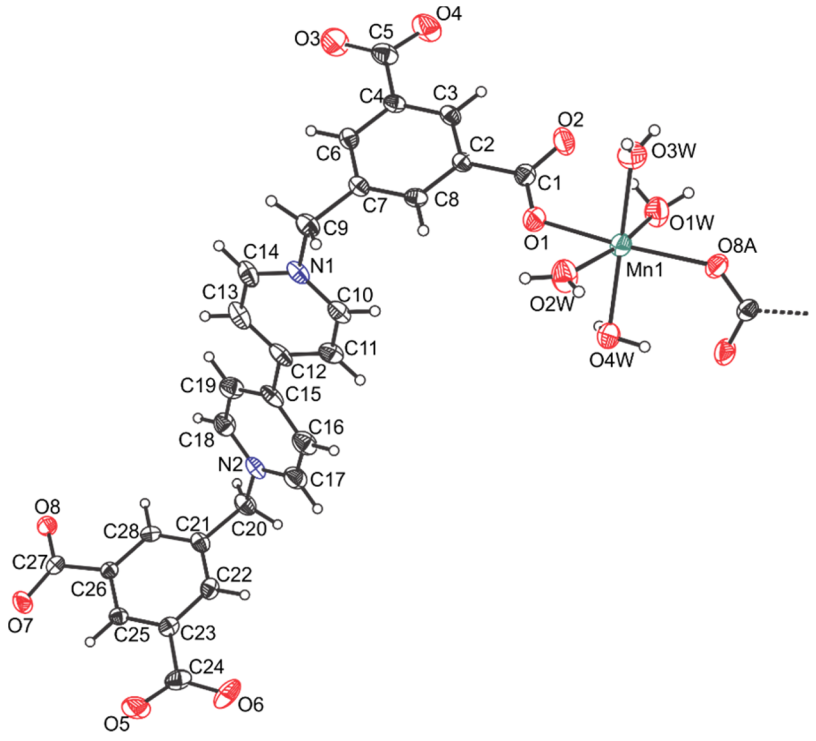

Figure 1. Crystal structure of $\{[Mn(bdcbpy)(OH_2)_4]\cdot 4H_2O\}_n$ (**1**) as a representative structure model for $\{[M(bdcbpy)(OH_2)_4]\cdot 4H_2O\}_n$ (M = Mn **1** and Ni **2**) with view of the coordination sphere of the manganese(II) cation with displacement ellipsoids drawn at the 50% probability level. Selected atoms are labeled. Symmetry code: A = $-x - 0.5, -y + 2.5, z + 0.5$. For ellipsoid plot of **2** see Supporting Information, Figure S5.

reacts with metal salts in aqueous solution to the new ZW MOFs $\{[Mn(bdcbpy)(OH_2)_4]\cdot 4H_2O\}_n$ (**1**) and $\{[Ni(bdcbpy)(OH_2)_4]\cdot 4H_2O\}_n$ (**2**) (Scheme 3). Similar reactions with other first-row transition metals were also attempted, but no further analogous compounds could be synthesized. Note that the ZW ligand $H_4bdcbpyBr_2$ is fully deprotonated in the framework, yielding the anionic ZW ligand $bdcbpy^{2-}$ bearing a total of two negative charges. This is sufficient to counterbalance M^{2+} metal clusters in MOFs, provided that metal-to-ligand ratios are 1:1, which is the case in **1** and **2**. To our best knowledge, $bdcbpy^{2-}$ is the first reported carboxylate-based ZW ligand bearing in total more than one negative charge. Ultimately, this approach allows the rational design of new pure ZW MOFs with no additional non-ZW anions being either incorporated in the framework or blocking pores.

Crystal Structures. The isostructural ZW MOFs $\{[M(bdcbpy)(OH_2)_4]\cdot 4H_2O\}_n$ (M = Mn **1** and Ni **2**) crystallize in the centrosymmetric monoclinic space group $P2_1/n$ with four formula units in the unit cell (Table 1). The asymmetric unit consists of one M(II) cation, one $bdcbpy^{2-}$ ligand, and eight water molecules, whereas three water molecules could not be refined and were removed from the electron density map using the SQUEEZE routine in Platon (see Experimental Section). All atoms are located in crystallographically independent

DOI: 10.1021/ic5026813
Inorg. Chem. 2015, 54, 1756−1764

general positions. In the crystal structure each M(II) cation is coordinated by two symmetry-related bdcbpy^{2-} ligands and four water molecules in an octahedral geometry (Figure 1).

The MO_6 octahedron is formed by six approximately equal M−O distances ranging from 2.158(2) to 2.232(2) Å in **1** and from 2.050(2) to 2.139(2) Å in **2**. The cis bond angles are in the range of 83.63(8)−93.01(7) in **1** and 84.34(6)−98.28(6) in **2**, while the trans bond angles are in the range of 168.25(8)−177.63(8)° in **1** and 173.08(6)−177.11(6)° in **2** (Table 2).

Table 2. Selected Bond Lengths [Å] and Angles [deg] for Compounds 1 and 2

	Mn **1**	Ni **2**
M−O1W	2.188(2)	2.055(2)
M−O2W	2.171(2)	2.061(2)
M−O3W	2.158(2)	2.050(2)
M−O4W	2.228(2)	2.099(2)
M−O1	2.177(2)	2.071(2)
M−O8A[a]	2.232(2)	2.139(2)
O3W−M−O1W	92.01(9)	92.60(6)
O3W−M−O2W	89.17(9)	88.37(6)
O1W−M−O2W	168.25(8)	173.08(6)
O3W−M−O1	91.90(8)	91.27(6)
O1W−M−O1	84.65(8)	88.79(6)
O2W−M−O1	83.63(8)	84.34(6)
O3W−M−O4W	177.63(8)	177.11(6)
O1W−M−O4W	90.33(8)	89.88(6)
O2W−M−O4W	88.63(8)	88.99(6)
O1−M−O4W	88.74(7)	87.30(5)
O3W−M−O8A	86.56(8)	86.99(6)
O1W−M−O8A	90.21(8)	88.61(6)
O2W−M−O8A	101.53(8)	98.28(6)
O1−M−O8A	174.57(8)	176.81(5)
O4W−M−O8A	93.01(7)	94.55(5)

[a]Symmetry code: A = $-x - 0.5, -y + 2.5, z + 0.5$.

Because the methylene groups are used as knots to link together the pyridine and phenyl rings, the whole bdcbpy^{2-} ligand is not linear and exhibits a zigzag conformation. The two pyridine rings of the 4,4′-bipyridyl group of the bdcbpy^{2-} ligand are slightly twisted with dihedral angles of 16.40(1)° in **1** and 18.01(1)° in **2**, while the phenyl rings are significantly twisted from the neighboring pyridine ring with dihedral angles of 69.69(1)/72.21(1)° in **1** and 70.19(1)/73.80(1)° in **2**. The two phenyl rings are almost aligned parallel, showing dihedral angles of 3.46(1)° in **1** and 3.25(1)° in **2**.

The metal ions are bridged by the bdcbpy^{2-} ligands to form 1D zigzag chains in a distorted linear relationship with M···M···M angles of 153.28(1)° in **1** and 152.78(1)° in **2**. Of four carboxylate groups in each bdcbpy^{2-} ligand, only two carboxylate groups bridge the metal centers in a monodentate coordination mode, whereas two carboxylate groups remain terminal nonbridging. Considering this behavior, the bdcbpy^{2-} ligand adopts an overall trans configuration of the two bridging carboxylate groups (Figure 2a). The lineal distances between the O atoms of the two bridging carboxylate groups amount to 16.804(1) Å in **1** and 16.807(1) Å in **2**, while intrachain metal−metal separations amount to 20.198(1) Å in **1** and 20.022(1) Å in **2**.

There exist one intramolecular and five intermolecular hydrogen bonds involving hydrogens of the coordinating water molecules and the nearest noncoordinating carboxylate O atoms around the metal centers (Table 3). Also, distinct aromatic $\pi-\pi$ stacking interactions can be found (Table 4). Taking all these extensive interchain interactions into account, the overall crystal packing can be regarded as a 3D supramolecular coordination network forming 1D channel pores along the crystallographic *a* axis with pore diameters of ∼3 Å (Figure 2c,d). In the as-synthesized structures, four noncoordinating water molecules occupy the pores. The smallest interchain separation of two metal cations amounts to 5.376(1) Å in **1** and 5.633(1) Å in **2**.

Thermal Properties. On heating the octahydrate $\{[Mn(bdcbpy)(OH_2)_4]\cdot 4H_2O\}_n$ (**1**), all water molecules can be removed. Two mass steps are observed in the TGA curve in the range of 30−300 °C that are each accompanied by an endothermic event in the DSC curve (Figure 3, upper). The TG steps are well-resolved and separated. The experimental mass losses of Δm_{exp}(1st step) = 9.9% and Δm_{exp}(2nd step) = 9.7% are in good agreement with that calculated for the release of each four water molecules [$\Delta m_{calc}(4H_2O)$ = 10.2%]. On the basis of the experimental mass losses, it can be assumed that in the first step the tetrahydrate $[Mn(bdcbpy)(OH_2)_4]_n$ is formed leading to the formation of the anhydrate $[Mn(bdcbpy)]_n$ (**1′**) upon further heating before it starts decomposing at ∼300 °C. The four noncoordinating water molecules are most likely released first, followed by the four coordinating water molecules, because of their strong hydrogen bonding interactions with the framework (Table 3).

As found from elemental analysis, $\{[Ni(bdcbpy)(OH_2)_4]\cdot 4H_2O\}_n$ (**2**) partially dehydrates instantly after synthesis and workup at room temperature. It can be assumed that one of the volatile noncoordinating water molecules leaves the framework giving a new composition of $\{[Ni(bdcbpy)(OH_2)_4]\cdot 3H_2O\}_n$. This heptahydrate shows a significantly different dehydration behavior than compound **1**. Three mass steps are observed in the TGA curve in the range of 30−300 °C that are each accompanied by an endothermic event in the DSC curve (Figure 3, lower). The experimental mass losses of Δm_{exp}(1st step) = 8.0%, Δm_{exp}(2nd step) = 7.4%, and Δm_{exp} = 3.1% (3rd step) are in good agreement with that calculated for the release of three water molecules in the 1st/2nd step [$\Delta m_{calc}(3H_2O)$ = 7.8%] and one water molecule in the third step [$\Delta m_{calc}(1H_2O)$ = 2.6%]. As with compound **1**, the noncoordinating water molecules are most likely released first before releasing the metal-coordinating water molecules. However, the next heating event in **2** is separated into two steps as compared to **1**. This observation can be explained based on the different metal−water coordination strengths and hydrogen bonding interactions. As shown in Table 2, the metal−O_{water} distances in **2** are significantly shorter with 2.050(2)−2.099(2) Å, as compared to those of **1** with 2.158(2)−2.228(2) Å, which indicates a stronger bonding in **2**. Also, as shown in Table 3 and Figure 2b, there are two metal-coordinating water molecules, namely, O1W and O4W, which are stabilized by two hydrogen bonding interactions and with O1W showing in average stronger hydrogen bonds than O4W, while O2W and O3W show instead only one hydrogen bond. This environment makes O1W the strongest-bonded water molecule in **2**, and thus, it can be assumed that this water molecule is released last upon heating. These energetic differences in the metal−water coordination are less pronounced in **1** and, thus, not resolved in the TGA curve of **1**. Heating rate-dependent TGA and DSC measurements of **1** showed no impact on the resolution of this heating step (Supporting Information, Figure S6).

DOI: 10.1021/ic5026813
Inorg. Chem. 2015, 54, 1756−1764

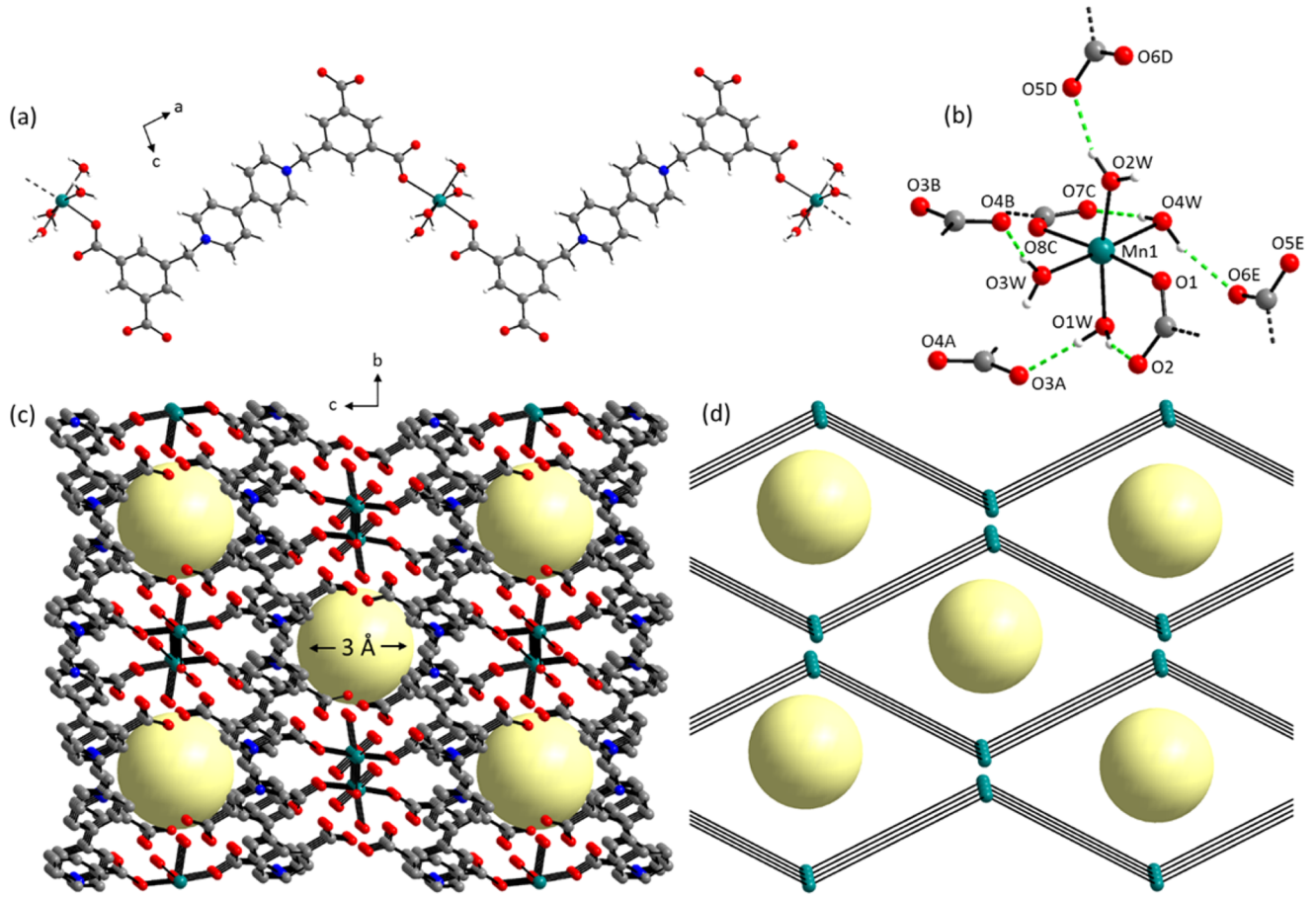

Figure 2. Crystal structure of $\{[Mn(bdcbpy)(OH_2)_4]\cdot 4H_2O\}_n$ (**1**) with view onto different motifs: (a) view onto a single chain; (b) coordination environment of a single metal cation with adjacent hydrogen bonded carboxylate groups, dashed green lines indicate interchain and intrachain hydrogen bonding (Table 3); (c) 3D supramolecular coordination network with view along the crystallographic *a* axis, yellow spheres represent potential solvent accessible voids, hydrogen atoms are omitted for the sake of clarity; (d) simplified framework with view along the crystallographic *a* axis, solid lines represent $bdcbpy^{2-}$ ligands.

Table 3. Characteristic Distances and Angles of Hydrogen Bonding Interactions in Compounds 1 and 2

D−H	*d*(H···A) [Å]	∠DHA [deg]	*d*(D···A) [Å]	A[a]
O1W−H1O1	1.857/1.874	177.04/175.54	2.696/2.712	O3A
O1W−H2O1	1.843/1.808	160.20/163.10	2.649/2.623	O2
O2W−H2O2	1.830/1.859	164.42/162.91	2.648/2.673	O5D
O3W−H2O3	1.861/1.887	165.42/162.22	2.683/2.699	O4B
O4W−H1O4	1.818/1.778	163.65/167.44	2.635/2.604	O7C
O4W−H2O4	1.917/1.947	165.87/164.90	2.739/2.767	O6E

[a]Symmetry codes: A = $x - 0.5, -y + 1.5, z - 0.5$; B = $-x - 1.5, y + 0.5, -z + 1.5$; C = $x - 1.5, -y + 1.5, z - 0.5$; D = $-x, -y + 2, -z + 1$; E = $x - 1, y, z$.

Table 4. Characteristic Distances of $\pi-\pi$ Stacking Interactions in Compounds 1 and 2

	d(ring···ring)[a] [Å]	∠ring planes[a] [deg]
ring1···ring3A[b]	3.810/3.812	14.6/18.3
ring1···ring4B	3.686/3.655	3.3/3.2
ring2···ring4C	3.648/3.636	5.7/5.8
ring3···ring1D	3.810/3.812	14.6/18.3
ring4···ring1E	3.686/3.655	3.3/3.2
ring4···ring2F	3.648/3.636	5.7/5.8

[a]Intermolecular face-to-face distances between the ring centroids of the six-membered rings and the angle between the ring planes are given. [b]Definitions: ring1 = C2−C3−C4−C6−C7−C8; ring2 = N1−C10−C11−C12−C13−C14; ring3 = C15−C16−C17−N2−C18−C19; ring4 = C21−C22−C23−C25−C26−C28; symmetry codes: A = $-x - 0.5, y + 0.5, -z + 1.5$; B = $x - 1, y, z$; C = $-x + 0.5, y + 0.5, -z + 1.5$; D = $-x - 0.5, y - 0.5, -z + 1.5$, E = $x + 1, y, z$; F = $-x + 0.5, y - 0.5, -z + 1.5$.

Removal of the water molecules causes a significant structural change in the frameworks of **1** and **2**. The PXRD analysis after complete dehydration by heating the as-synthesized compounds **1** and **2** at 100 °C for 12 h shows a significant loss in crystallinity and that the reflections have mostly vanished and are significantly different from those of the initial sample (Figure 4).

This reveals the formation of new anhydrate phases $[M(bdcbpy)]_n$ M = Mn **1′** and Ni **2′**. However, upon exposure to regular laboratory air at room temperature for 3 h, the diffraction intensities have obviously increased, and their PXRD patterns (Figure 4) and TGA curves (Supporting Information, Figure S7) match well with those of **1** and **2**. This reveals that the anhydrates **1′** and **2′** rehydrate to the as-synthesized forms **1** and **2** and regain their crystallinity completely, thus indicating that the process is reversible.

Adsorption Properties. Gas-adsorption measurements at 77 K reveal that both compounds have no affinity to N_2. Further adsorption experiments with CO_2 at 195 K show no

DOI: 10.1021/ic5026813
Inorg. Chem. 2015, 54, 1756−1764

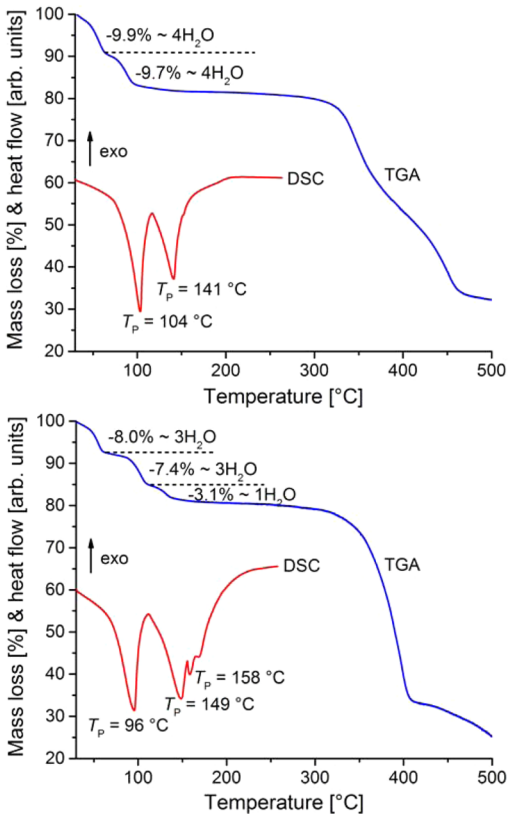

Figure 3. TGA and DSC curves for compounds **1** (upper) and **2** (lower). Heating rate = 3 °C·min^{-1}; given are the peak temperatures T_P [°C]. For heating rate-dependent TG and DCS investigations see Supporting Information, Figure S6.

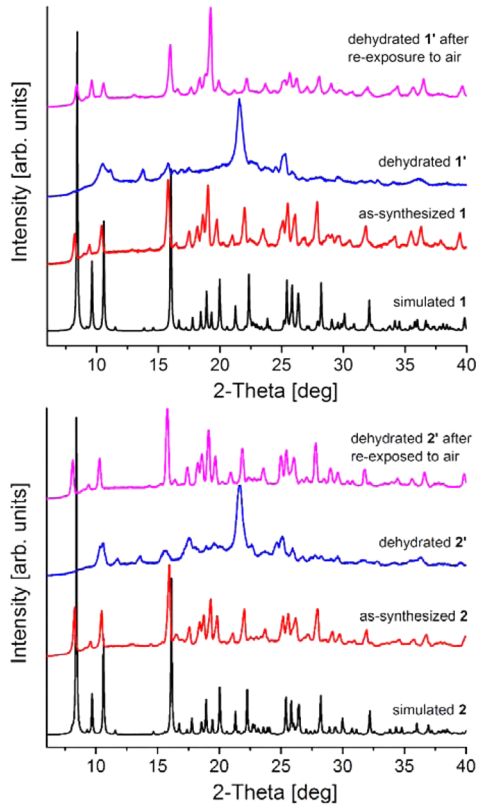

Figure 4. Powder X-ray diffraction patterns for simulated, as-synthesized, dehydrated, and dehydrated samples exposed to air for 1 h of compounds **1** (upper) and **2** (lower). Please note that intensities of simulated and experimental patterns do not match due to preferred orientation of the bulk material.

significant uptake. However, a H_2 adsorption of 8.6 cm^3/g for **1** and 11.6 cm^3/g for **2** can be observed, which can be regarded as a significant uptake capacity taking the potential void space of only 13.2% for **1** and 18.0% for **2** into account (Figure 5). Although it is not among those with the highest H_2 uptake, the positive slope at 1 bar, which is an indication of unsaturation, shows that they may have higher hydrogen uptake capacities under higher pressures.

The van der Waals accessible pore sizes can be estimated from single-crystal data to be ~3 Å for both hydrated as-synthesized materials **1** and **2**. However, even smaller pore sizes are expected for the dehydrated activated materials, assuming that the removal of coordinating water molecules, as shown in Figure 2b, cause adjacent carboxylate oxygen atoms to coordinate to the metal centers. This transition would retain the overall octahedral coordination environment of the metals but would also lead to an even tighter framework as compared to the as-synthesized materials. Thus, on the basis of the aforementioned explanation, it can be assumed that N_2 and CO_2 show no adsorption due to size exclusion in respect to their kinetic diameters of 3.64 and 3.3 Å, respectively, whereas H_2 with a kinetic diameter of 2.89 Å can diffuse into the <3 Å narrow pores.

Photochromic Properties. Both compounds **1** and **2** are very photosensitive, giving a visible color change within seconds upon exposure to UV light (365 nm, 100 W, UVP B-100AP) in air. Compound **1** turns from ivory to dark blue, while compound **2** changes from light green to dark green (Figure 6). This color change is similar to that observed for viologen radicals,[40−46] suggesting that the color change of **1** and **2** may

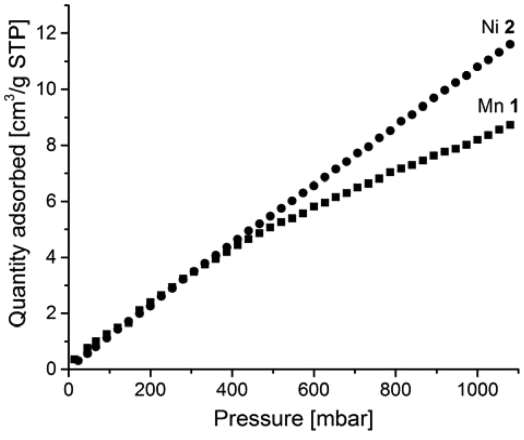

Figure 5. Hydrogen adsorption isotherms collected at 77 K of **1** (squares) and **2** (circles).

arise from the photostimulated reduction of the bdcbpy^{2-} ligand to generate bdcbpy$^{\bullet 3-}$ radicals after the compounds are irradiated. Investigations on the reversibility of this process have shown that **1** and **2** transform to their nonradical states within 10 min in air over several continuous cycles without noticeable loss in the ability to generate free radicals. This reversible transformation can be explained by a process of oxidative quenching from bdcbpy$^{\bullet 3-}$ radicals to bdcbpy^{2-} by O_2 as found in common photoreduced products of viologen derivatives.[67] In the course of these investigations we noticed that **1** retains its single-crystallinity upon radical formation,

DOI: 10.1021/ic5026813
Inorg. Chem. 2015, 54, 1756−1764

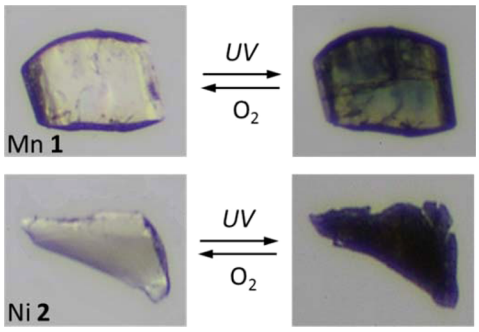

Figure 6. Photochromic effect of single-crystalline samples of compounds **1** (upper) and **2** (lower) shown as photographic images. Photographs of polycrystalline samples are shown in Supporting Information, Figure S8.

whereas **2** transforms to a polycrystalline state (Figure 6). This observation might be explained through different transformation reaction mechanisms. It can be assumed that the radical formation of **1** proceeds via a topotactic reaction, whereas **2** undergoes a significant rearrangement of its structure via a nontopotactic reaction.

To get further insights into the influence of the structure on the photochromic behavior, the interchain packing interactions of the bdcbpy^{2-} ligand were analyzed (Figure 7, Table 5). The

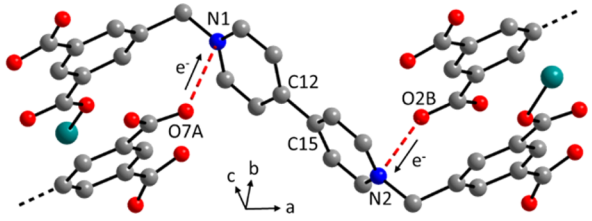

Figure 7. Orientation of the bdcbpy^{2-} ligand in compound **1** as representative for both isostructural compounds **1** and **2**. Potential interchain electron transfer routes and selected atoms are labeled; distances and angles between selected atoms are given in Table 5.

Table 5. Interchain Distances [Å] and Angles [deg] between Selected Atoms as Labeled in Figure 7

	Mn **1**	Ni **2**
N1···O7A[a]	3.385	3.438
N2···O2B	3.439	3.515
O7A···N1···C12	65.0	63.1
O2B···N2···C15	70.9	71.0

[a]Symmetry codes: A = $x - 1$, y, z and B = $x + 1$, y, z.

shortest distances between the carboxylate O atoms and pyridinium nitrogen atoms are 3.385 Å in **1** and 3.438 Å in **2**, while being roughly perpendicular to each other with angles of 65.0° in **1** and 63.1° in **2**. Such geometries and distances are suitable for the occurrence of photoinduced electron transfer reactions between the bipyridinium acceptor units and carboxylate donor groups to generate radicals.[40−46]

CONCLUSION

With this contribution we employed a new design strategy to rationally synthesize ZW MOF materials. Through a careful structural analysis of reported porous ZW MOF materials we found that either their potential pores are blocked by charge-compensating anions or that charge-compensating ions are incorporated into the frameworks. The latter situation has shown to yield compounds in which only heterogeneous pore linings are found showing a mixture of charged organic surfaces and noncharged organic surfaces. To allow the formation of materials showing pores with homogeneously charged pore linings we designed the multicharged anionic ZW ligand bdcbpy^{2-}, which has been successfully used to construct the isostructural ZW MOFs Mn **1** and Ni **2** with no additional anions needed for the charge-compensation purpose. The formation of their crystal structures demonstrates spontaneous self-assembly reactions involving three types of molecular recognition phenomena, namely, metal-ion recognition in the first step, hydrogen bonding in the second step, and $\pi-\pi$ stacking interactions in the final step to establish a 3D framework with 1D channel pores. The compounds were thoroughly investigated for their adsorption properties, thermostabilty, and activation conditions. In addition, an interesting photochromic behavior was found upon UV light irradiation, which originated through the formation of viologen radicals. Although the presented materials are not among those with the highest hydrogen uptake, this work is the first example of ZW MOFs formed solely through ZW ligands and no other charge-balancing anions. Thus, this research will open new avenues for the rational design of advanced porous ZW MOFs with enhanced adsorption properties. Further studies on creating similar materials based on anionic ZW ligands are in progress.

ASSOCIATED CONTENT

Supporting Information

NMR data of Me_4bdcbpyBr$_2$ and H_4bdcbpyBr$_2$; IR data of H_4bdcbpyBr$_2$, **1**, and **2**; PXRD data of **1** and **2**; temperature ellipsoid plot of **2**; heating rate-dependent TGA and DSC data of **1** and **2**; TGA data of rehydrated samples of **1** and **2**; photographic images of the photochromic effect of polycrystalline samples of **1** and **2**. This material is available free of charge via the Internet at http://pubs.acs.org. CCDC 1031541 (**1**) and 1031542 (**2**) contain the supplementary crystallographic data for this paper. These data can be obtained free of charge from the Cambridge Crystallographic Data Centre via www.ccdc.cam.ac.uk.

AUTHOR INFORMATION

Corresponding Author

*Phone: +1 (315) 268-2355. Fax: +1 (315) 268-6610. E-mail: mwriedt@clarkson.edu.

Notes

The authors declare no competing financial interest.

ACKNOWLEDGMENTS

We thank Clarkson University for their generous start-up funding.

REFERENCES

(1) Dincă, M.; Long, J. R. *Angew. Chem., Int. Ed.* **2008**, *47*, 6766−6779.
(2) He, Y.; Zhou, W.; Qian, G.; Chen, B. *Chem. Soc. Rev.* **2014**, *43*, 5657−78.
(3) Suh, M. P.; Park, H. J.; Prasad, T. K.; Lim, D.-W. *Chem. Rev.* **2011**, *112*, 782−835.
(4) Ramaswamy, P.; Wong, N. E.; Shimizu, G. K. H. *Chem. Soc. Rev.* **2014**, *43*, 5913−32.
(5) Zhang, T.; Lin, W. *Chem. Soc. Rev.* **2014**, *43*, 5982−93.

DOI: 10.1021/ic5026813
Inorg. Chem. 2015, 54, 1756−1764

(6) Long, J. R.; Yaghi, O. M. *Chem. Soc. Rev.* **2009**, *38*, 1201−1508 all articles of this special issue.
(7) Zhou, H.-C.; Long, J. R.; Yaghi, O. M. *Chem. Rev.* **2012**, *112*, 673−1268 all articles of this special issue.
(8) Stavila, V.; Talin, A. A.; Allendorf, M. D. *Chem. Soc. Rev.* **2014**, *43*, 5994−6010.
(9) Gao, W.-Y.; Chrzanowski, M.; Ma, S. *Chem. Soc. Rev.* **2014**, *43*, 5841−66.
(10) Hu, Z.; Deibert, B. J.; Li, J. *Chem. Soc. Rev.* **2014**, *43*, 5815−40.
(11) Zhou, H.-C.; Kitagawa, S. *Chem. Soc. Rev.* 2014, *43*, all articles of this special issue.
(12) Hu, Y.; Verdegaal, W. M.; Yu, S.-H.; Jiang, H.-L. *ChemSusChem* **2014**, *7*, 734−737.
(13) Zhou, Y.-X.; Chen, Y.-Z.; Hu, Y.; Huang, G.; Yu, S.-H.; Jiang, H.-L. *Chem.—Eur. J.* **2014**, *20*, 14976−14980.
(14) Wriedt, M.; Sculley, J. P.; Yakovenko, A. A.; Ma, Y.; Halder, G. J.; Balbuena, P. B.; Zhou, H.-C. *Angew. Chem., Int. Ed.* **2012**, *51*, 9804−9808.
(15) Sculley, J. P.; Verdegaal, W. M.; Lu, W.; Wriedt, M.; Zhou, H.-C. *Adv. Mater.* **2013**, *25*, 3957−3961.
(16) Wriedt, M.; Sculley, J. P.; Verdegaal, W. M.; Yakovenko, A. A.; Zhou, H.-C. *Chem. Commun.* **2013**, *49*, 9612−9614.
(17) Xiong, S.; He, Y.; Krishna, R.; Chen, B.; Wang, Z. *Cryst. Growth Des.* **2013**, *13*, 2670−2674.
(18) Couck, S.; Denayer, J. F. M.; Baron, G. V.; Rémy, T.; Gascon, J.; Kapteijn, F. *J. Am. Chem. Soc.* **2009**, *131*, 6326−6327.
(19) Li, H.; Feng, X.; Guo, Y.; Chen, D.; Li, R.; Ren, X.; Jiang, X.; Dong, Y.; Wang, B. *Sci. Rep.* **2014**, *4*, 4366.
(20) Guo, Z.; Wu, H.; Srinivas, G.; Zhou, Y.; Xiang, S.; Chen, Z.; Yang, Y.; Zhou, W.; O'Keeffe, M.; Chen, B. *Angew. Chem., Int. Ed.* **2011**, *50*, 3178−3181.
(21) Kong, X.; Scott, E.; Ding, W.; Mason, J. A.; Long, J. R.; Reimer, J. A. *J. Am. Chem. Soc.* **2012**, *134*, 14341−14344.
(22) Pham, T.; Forrest, K. A.; Nugent, P.; Belmabkhout, Y.; Luebke, R.; Eddaoudi, M.; Zaworotko, M. J.; Space, B. *J. Phys. Chem. C* **2013**, *117*, 9340−9354.
(23) Moss, G. P.; Smith, P. A. S.; Tavernier, D. *Pure Appl. Chem.* **1995**, *67*, 1307.
(24) Destro, R.; Roversi, P.; Barzaghi, M.; Marsh, R. E. *J. Phys. Chem. A* **2000**, *104*, 1047−1054.
(25) LeSar, R.; Herschbach, D. R. *J. Phys. Chem.* **1983**, *87*, 5202−5206.
(26) Bae, Y. S.; Lee, C. H. *Carbon* **2005**, *43*, 95−107.
(27) Welton, T. *Chem. Rev.* **1999**, *99*, 2071−2084.
(28) Dupont, J.; de Souza, R. F.; Suarez, P. A. Z. *Chem. Rev.* **2002**, *102*, 3667−3692.
(29) Miao, W.; Chan, T. H. *Acc. Chem. Res.* **2006**, *39*, 897−908.
(30) Wang, X.-W.; Han, L.; Cai, T.-J.; Zheng, Y.-Q.; Chen, J.-Z.; Deng, Q. *Cryst. Growth Des.* **2007**, *7*, 1027−1030.
(31) Wu, A. Q.; Li, Y.; Zheng, F.-K.; Guo; Huang, J.-S. *Cryst. Growth Des.* **2005**, *6*, 444−450.
(32) Ma, Y.; Li, X.-B.; Yi, X.-C.; Jia, Q.-X.; Gao, E.-Q.; Liu, C.-M. *Inorg. Chem.* **2010**, *49*, 8092−8098.
(33) Chen, J.-X.; Lin, W.-E.; Zhou, C.-Q.; Yau, L. F.; Wang, J.-R.; Wang, B.; Chen, W.-H.; Jiang, Z.-H. *Inorg. Chim. Acta* **2011**, *376*, 389−395.
(34) Kong, G.-Q.; Wu, C.-D. *Cryst. Growth Des.* **2010**, *10*, 4590−4595.
(35) Sun, Y.-Q.; Zhang, J.; Ju, Z.-F.; Yang, G.-Y. *Cryst. Growth Des.* **2005**, *5*, 1939−1943.
(36) Yao, Q.-X.; Jin, X.-H.; Ju, Z.-F.; Zhang, H.-X.; Zhang, J. *CrystEngComm* **2009**, *11*, 1502−1504.
(37) Sun, J.-K.; Cai, L.-X.; Chen, Y.-J.; Li, Z.-H.; Zhang, J. *Chem. Commun.* **2011**, *47*, 6870−6872.
(38) Li, Y.; Li, G.-Q.; Zou, W.-Q.; Zheng, F.-K.; Zou, J.-P.; Guo, G.-C.; Lu, C.-Z.; Huang, J.-S. *J. Mol. Struct.* **2007**, *837*, 231−236.
(39) Sun, J.-K.; Wang, P.; Yao, Q.-X.; Chen, Y.-J.; Li, Z.-H.; Zhang, Y.-F.; Wu, L.-M.; Zhang, J. *J. Mater. Chem.* **2012**, *22*, 12212−12219.
(40) Fu, K.; Ren, C.-X.; Chen, C.; Cai, L.-X.; Tan, B.; Zhang, J. *CrystEngComm* **2014**, *16*, 5134−5141.
(41) Jin, X.-H.; Sun, J.-K.; Xu, X.-M.; Li, Z.-H.; Zhang, J. *Chem. Commun.* **2010**, *46*, 4695−4697.
(42) Sun, J.-K.; Wang, P.; Chen, C.; Zhou, X.-J.; Wu, L.-M.; Zhang, Y.-F.; Zhang, J. *Dalton Trans.* **2012**, *41*, 13441−13446.
(43) Tan, Y.; Chen, H.; Zhang, J.; Liao, S.; Dai, J.; Fu, Z. *CrystEngComm* **2012**, *14*, 5137−5139.
(44) Tan, Y.; Fu, Z.; Zeng, Y.; Chen, H.; Liao, S.; Zhang, J.; Dai, J. *J. Mater. Chem.* **2012**, *22*, 17452−17455.
(45) Yao, Q.-X.; Ju, Z.-F.; Jin, X.-H.; Zhang, J. *Inorg. Chem.* **2009**, *48*, 1266−1268.
(46) Zeng, Y.; Liao, S.; Dai, J.; Fu, Z. *Chem. Commun.* **2012**, *48*, 11641−11643.
(47) Higuchi, M.; Nakamura, K.; Horike, S.; Hijikata, Y.; Yanai, N.; Fukushima, T.; Kim, J.; Kato, K.; Takata, M.; Watanabe, D.; Oshima, S.; Kitagawa, S. *Angew. Chem., Int. Ed.* **2012**, *51*, 8369−8372.
(48) Higuchi, M.; Tanaka, D.; Horike, S.; Sakamoto, H.; Nakamura, K.; Takashima, Y.; Hijikata, Y.; Yanai, N.; Kim, J.; Kato, K.; Kubota, Y.; Takata, M.; Kitagawa, S. *J. Am. Chem. Soc.* **2009**, *131*, 10336−10337.
(49) Lin, J.-B.; Shimizu, G. K. H. *Inorg. Chem. Front.* **2014**, *1*, 302−305.
(50) Sun, J.-K.; Ji, M.; Chen, C.; Wang, W.-G.; Wang, P.; Chen, R.-P.; Zhang, J. *Chem. Commun.* **2013**, *49*, 1624−1626.
(51) Yao, Q.-X.; Pan, L.; Jin, X.-H.; Li, J.; Ju, Z.-F.; Zhang, J. *Chem.—Eur. J.* **2009**, *15*, 11890−11897.
(52) Kanoo, P.; Matsuda, R.; Sato, H.; Li, L.; Jeon, H. J.; Kitagawa, S. *Inorg. Chem.* **2013**, *52*, 10735−10737.
(53) Sun, J.-K.; Yao, Q.-X.; Tian, Y.-Y.; Wu, L.; Zhu, G.-S.; Chen, R.-P.; Zhang, J. *Chem.—Eur. J.* **2012**, *18*, 1924−1931.
(54) Humphrey, S. M.; Allan, P. K.; Oungoulian, S. E.; Ironside, M. S.; Wise, E. R. *Dalton Trans.* **2009**, 2298−2305.
(55) Ibarra, I. A.; Tan, K. E.; Lynch, V. M.; Humphrey, S. M. *Dalton Trans.* **2012**, *41*, 3920−3923.
(56) Lalonde, M. B.; Getman, R. B.; Lee, J. Y.; Roberts, J. M.; Sarjeant, A. A.; Scheidt, K. A.; Georgiev, P. A.; Embs, J. P.; Eckert, J.; Farha, O. K.; Snurr, R. Q.; Hupp, J. T. *CrystEngComm* **2013**, *15*, 9408−9414.
(57) Barman, S.; Furukawa, H.; Blacque, O.; Venkatesan, K.; Yaghi, O. M.; Berke, H. *Chem. Commun.* **2010**, *46*, 7981−7983.
(58) Barman, S.; Khutia, A.; Koitz, R.; Blacque, O.; Furukawa, H.; Iannuzzi, M.; Yaghi, O. M.; Janiak, C.; Hutter, J.; Berke, H. *J. Mater. Chem. A* **2014**, *2*, 18823−18830.
(59) Huang, X.; Huang, S.; Zhai, B.; Zhang, Y.; Xu, Y.; Wang, Q. *Tetrahedron Lett.* **2012**, *53*, 6414−6417.
(60) *SAINT and APEX 2 Software for CCD Diffractometers;* Bruker AXS Inc.: Madison, WI, 2014.
(61) Sheldrick, G. M. *SADABS, version 2014/4;* Bruker AXC Inc.: Madison, WI, 2014.
(62) Sheldrick, G. M. *Acta Crystallogr.* **2008**, *A64*, 112−122.
(63) Sheldrick, G. M. *SHELXT;* University of Göttingen: Germany, 2014.
(64) Sheldrick, G. M. *SHELXL;* University of Göttingen: Germany, 2014.
(65) Spek, A. L. *Acta Crystallogr., Sect. D* **2009**, *65*, 148−155.
(66) Macrae, C. F.; Bruno, I. J.; Chisholm, J. A.; Edgington, P. R.; McCabe, P.; Pidcock, E.; Rodriguez-Monge, L.; Taylor, R.; van de Streek, J.; Wood, P. A. *J. Appl. Crystallogr.* **2008**, *41*, 466−470.
(67) Monk, P. M. S. *The Viologens: Physicochemical Properties, Synthesis and Applications of the Salts of 4,4′-Bipyridine;* John Wiley & Sons: New York, 1999.

DOI: 10.1021/ic5026813
Inorg. Chem. 2015, 54, 1756−1764